



## Adsorption efficiency of batik dye by modified *Dialium cochinchinense* activated carbon beads: kinetics and thermodynamics

Fareeda Hayeeye<sup>a</sup>, Aeesoh Benhawan<sup>b</sup>, Memoon Sattar<sup>c,\*</sup>

<sup>a</sup>Department of Science, Faculty of Science and Technology, Prince of Songkla University, Pattani Campus, Thailand, email: fareeda.ha@psu.ac.th

<sup>b</sup>Department of Chemistry, Faculty of Science Technology and Agriculture, Yala Rajabhat University, Thailand, email: aeesoh.b@yru.ac.th

<sup>c</sup>Faculty of Sports and Health Science, Thailand National Sports University, Yala Campus, Thailand, Tel. (+66) 0855812146; email: memoonsattar@gmail.com

Received 5 November 2021; Accepted 14 July 2022

### ABSTRACT

*Dialium cochinchinense* seeds as local agricultural waste were used with two preparation methods to create new adsorbents: *Dialium cochinchinense* seed activated carbon (DCS-AC); and a bead form composite of poly(lactic acid)/*Dialium cochinchinense* seed powder activated carbon (PLA/DCS-AC). The target was an eco-friendly, bio-degradable, inexpensive material for the treatment of wastewater from batik dyeing. Brunauer–Emmett–Teller surface area, scanning electron microscopy images, Fourier-transform infrared spectra, and the point of zero charge ( $\text{pH}_{\text{pzc}}$ ) were assessed. The effects of contact time, adsorbent dosage, pH, and temperature were examined and the Langmuir adsorption isotherm fit well. The calculated maximum adsorption capacities ( $q_m$ ) were 222.22 and 147.06  $\text{mg g}^{-1}$  for DCS-AC and PLA/DCS-AC, respectively. The adsorption process was endothermic and spontaneous. Moreover, the desorption study confirmed that DCS-AC and PLA/DCS-AC can be regenerated. The batch adsorption of batik dye by DCS-AC and PLA/DCS-AC adsorbents appears an efficient approach to wastewater treatment.

**Keywords:** Adsorption isotherm; Batik process; *Dialium cochinchinense* seed activated carbon; Poly(lactic acid)

### 1. Introduction

In the three southern border provinces of Thailand, batik dyeing is a local traditional trade passed down from generation to generation. This industry has become highly commercialized and has contributed positively to economic growth. Moreover, this industry has become associated with Malay culture in the three southernmost provinces of Thailand, and attracts foreign and local tourists. High skills and the right equipment and tools are required to produce high quality batiks [1]. Generally, the effluent from the batik industry contains synthetic dyes, which are

loaded with heavy metals and are also carcinogenic. Dyes are the main constituents in the wastewater discharge, and they are of synthetic origin with complex aromatic molecular structures, and are classified as follows: anionic-direct, acidic and reactive dyes, cationic-based dyes, and non-ionic-disperse dyes [2]. Reactive dyes were used for batik dyeing, and they were usually azo-based chromophores in combination with various types of reactive groups such as vinyl sulfone, chlorotriazine, trichloropyrimidine, and difluorochloropyrimidine [3]. The dyes had strong effects on aquatic organisms, and the high chemical

\* Corresponding author.

oxygen demand (COD) and biological oxygen demand (BOD) indicated that the spring water was very low in oxygen [4], so it was necessary to treat the wastewater. There are many methods of wastewater treatment, such as photocatalysis, coagulation and membrane separation [5–7]. However, adsorption by activated carbon is commonly used to remove pollutants in wastewater treatment [8]. In previous studies, the adsorption of dyes has been tested with activated carbon prepared from various agricultural waste materials, such as rice husks, potato peels, pericarp of fruits, and almond shells [9–12]. Adsorption of Reactive Red 120 by activated carbon, including biosorption, has been investigated in many studies, but the adsorption capacities have remained low [13–15]. Thus, this study prepared novel adsorbents from *Dialium cochinchinense* seeds for Reactive Red 120 adsorption. The Reactive Red 120 molecular formula is  $C_{44}H_{24}Cl_2N_{14}Na_6O_{20}S_6$ , molecular weight  $1,470 \text{ g mol}^{-1}$ , and water solubility  $70 \text{ g L}^{-1}$ . The chemical structure of Reactive Red 120 is presented in Fig. 1. *Dialium cochinchinense* is an economic plant cultivated in Pattani Province of Thailand. This cultivation produces a lot of waste seeds, so *Dialium cochinchinense* seed waste was selected for the production of the new natural adsorbent *Dialium cochinchinense* seed activated carbon (DCS-AC) to be tested for replacing expensive commercial activated carbon. In addition, DCS-AC powder was compacted with poly(lactic acid) (PLA) by a simple phase inversion technique to form an efficient granular adsorbent, using N-methyl-2-pyrrolidone (NMP) and water as the solvent and the non-solvent, respectively. PLA was selected because it is a biodegradable, environmentally friendly, thermoplastic aliphatic polyester derived from renewable resources [16–17]. The aims of the study were to characterize the two new adsorbents (DCS-AC and PLA/DCS-AC) by iodine number, scanning electron microscopy (SEM) images, Brunauer–Emmett–Teller (BET) surface area and pore-size distribution, Fourier-transform infrared (FT-IR) spectra, and the point of zero charge ( $\text{pH}_{\text{pzc}}$ ); and to optimize various factors such as contact time, pH, and adsorbent dose; and evaluate the kinetic adsorption isotherms of Reactive Red 120 on DCS-AC and PLA/DCS-AC. The novel adsorbents offer advantages, convenience and high adsorption capacity for adsorption of the dye. Moreover, they are environmentally friendly alternative adsorbents for the wastewater treatment.

## 2. Materials and methods

### 2.1. Materials and reagents

*Dialium cochinchinense* seeds were procured from Yarung in Pattani Province. Zinc chloride ( $\text{ZnCl}_2$ ), phosphoric acid ( $\text{H}_3\text{PO}_4$ ) and potassium hydroxide (KOH) were obtained from Sigma-Aldrich. Sodium hydroxide (NaOH) and hydrochloric acid (HCl) used for pH adjustment were obtained from Labscan Ireland and Merck, respectively. PLA and NMP were purchased from NatureWorks (USA) and RCI Labscan Limited (Thailand), respectively. The adsorbate (Reactive Red 120) was purchased from Sigma-Aldrich. Reactive Red 120 stock solution at  $1,000 \text{ mg L}^{-1}$  was diluted with distilled water to obtain standard solutions

with Reactive Red 120 concentrations ranging from 50 to  $600 \text{ mg L}^{-1}$  for adsorption isotherm studies.

### 2.2. Preparation of DCS-AC and PLA/DCS-AC

*Dialium cochinchinense* seeds (DCS) were washed and oven-dried at  $120^\circ\text{C}$ . The carbonization was carried out in a muffle furnace at  $400^\circ\text{C}$  for 3 h. Then, mixing the char (DCS) with different chemical reagents for activation ( $\text{H}_3\text{PO}_4$ , KOH, and  $\text{ZnCl}_2$ ) was carried out at varied ratios of char to chemical reagents namely 1:0.5, 1:1.0, 1:1.5, 1:2.0, 1:2.5, and 1:3.0, at different temperatures ( $400^\circ\text{C}$ ,  $450^\circ\text{C}$  and  $500^\circ\text{C}$ ) for 1.0 h in the muffle furnace. Then, the obtained activated carbon was washed with distilled water to neutral pH. Finally, it was dried in an oven at  $110^\circ\text{C}$  for 24 h and stored in a desiccator.

PLA/DCS-AC beads were prepared by the phase inversion method as follows. A 10% PLA solution was prepared in NMP. DCS-AC was crushed and 5% w/v DCS-AC was added to the PLA solution and stirred for 24 h at room temperature. The homogeneous suspension was dropped into the non-solvent (distilled water) and it immediately formed beads. Then, the PLA/DCS-AC beads were washed several times with doubly distilled water and finally were dried in an oven for 6 h at  $60^\circ\text{C}$  [18].

### 2.3. Characterization of DCS-AC and PLA/DCS-AC

DCS-AC and PLA/DCS-AC were characterized by scanning electron microscopy (SEM-Quanta 400), for BET surface area and pore-size distribution (Model Autosorb 1 MP Quantachrome Instruments, FL, USA), for elemental composition (FLASH EA 112 Elemental Analyzer), and for FT-IR spectra in ATR mode (Spectrum GX, Perkin Elmer, USA) at the Scientific Equipment Center of the Prince of Songkla University. In addition, the iodine number and point of zero charge ( $\text{pH}_{\text{pzc}}$ ) were investigated according to ASTM D4607-94 [19] and the pH drift method [20], respectively.

The procedure for determining the iodine number was as follows. An 0.1 g sample of the adsorbent was mixed with 10 mL of 5% HCl in an Erlenmeyer flask until all the adsorbent was wetted. The suspension was then boiled for exactly 30 s and then it was cooled to room temperature. Then 100 mL of a 0.05 M standard iodine solution was added to the conical flask. This suspension was filtered using a Whatman 2 V filter paper and 50 mL of the filtrate was titrated with 0.1 M sodium thiosulfate until its yellow color almost disappeared. 1 mL of starch indicator was added and the titration was continued until the blue color just disappeared. The equilibrium concentration was determined by calculation of the amount of sodium thiosulfate used in the titration. The procedure was repeated with each adsorbent [19].

The point of zero charge was determined as follows. A 50 mL aliquot of a 0.1 M NaCl solution was adjusted with 0.1 M HCl or 0.1 M NaOH to a pH between 2 and 12; DCS-AC was added to each of the pH-adjusted solutions and allowed to equilibrate for 24 h; the final pH was measured and initial pH ( $\text{pH}_i$ ) and the final pH ( $\text{pH}_f$ ) were plotted. The intersection point of the curves where  $\text{pH}_i = \text{pH}_f$

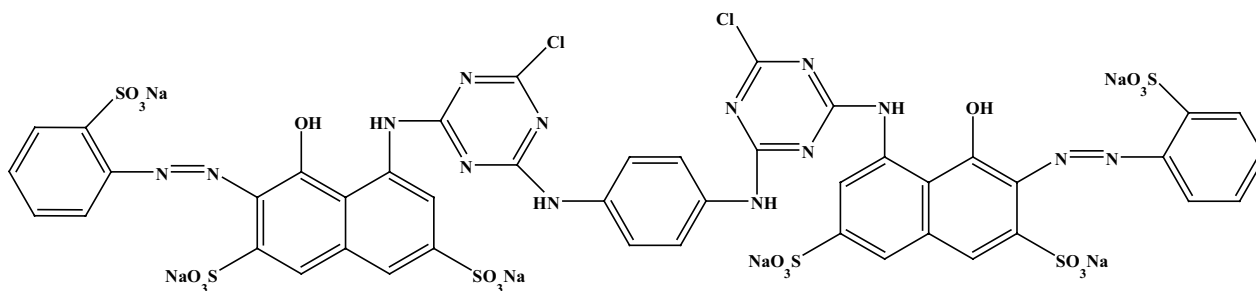


Fig. 1. Chemical structure of Reactive Red 120.

was taken as the  $\text{pH}_{\text{pzc}}$  of DCS-AC [21]. The above steps were repeated using PLA/DCS-AC.

#### 2.4. Adsorption studies

DCS-AC activated with  $\text{H}_3\text{PO}_4$  at a ratio of 1:1.5 at  $450^\circ\text{C}$  for 1 h gave the highest iodine number. Therefore, this adsorbent was selected for the adsorption tests of Reactive Red 120. In addition, the adsorption of Reactive Red 120 on PLA/DCS-AC was also investigated. In the batch adsorption method [22], 0.05 g of the adsorbent (DCS-AC or PLA/DCS-AC) was added to 50 mL of a solution with 50–600  $\text{mg L}^{-1}$  of Reactive Red 120, and the mixtures were stirred in a shaking bath at  $30^\circ\text{C}$ . The concentrations of Reactive Red 120 before and after adsorption were determined using a UV-Vis spectrophotometer at 536 nm wavelength. The residual dye concentration was calculated based on a previously determined calibration curve. The percentage removal of Reactive Red 120 (%RE) and the adsorption capacity,  $q_e$  ( $\text{mg g}^{-1}$ ), of the adsorbent were calculated using Eqs. (1) and (2), respectively [23]:

$$\% \text{RE} = \frac{C_0 - C_e}{C_0} \times 100 \quad (1)$$

$$q_e = \frac{V(C_0 - C_e)}{W} \quad (2)$$

where  $V$  is the volume of the solution (L),  $W$  is the mass of adsorbent (g), and  $C_0$  and  $C_e$  are the initial and equilibrium liquid-phase concentrations of Reactive Red 120 ( $\text{mg L}^{-1}$ ), respectively.

In addition, the effects of various parameters were also studied: the amount of DCS-AC and PLA/DCS-AC (0.1–0.6 g), contact time (0–48 h), and pH (2–11). All adsorption experiments on the different effects were performed with 50 mL of 100  $\text{mg L}^{-1}$  Reactive Red 120 solution at pH 5, the natural pH of the Reactive Red 120 solution. Moreover, all experiments were performed in triplicate. As regards the effects of pH, the initial pH of the Reactive Red 120 solutions was adjusted using HCl or NaOH solutions. Furthermore, the equilibrium data were evaluated using kinetic adsorption models (pseudo-first-order and pseudo-second-order models) and the most commonly used adsorption isotherms (Langmuir, Freundlich, Temkin and Dubinin–Radushkevich models).

### 3. Results and discussion

#### 3.1. Influence of preparation of DCS-AC

Table 1 shows the influences of impregnation ratio and activation reagents at different temperatures, and the DCS activated with  $\text{H}_3\text{PO}_4$  had a higher iodine number than those activated with KOH or  $\text{ZnCl}_2$ . Moreover, the impregnation ratio of DCS to  $\text{H}_3\text{PO}_4$  at 1:1.5 gave the highest iodine number (893.21  $\text{mg g}^{-1}$ ) at  $500^\circ\text{C}$ , while the iodine number slightly decreased at  $450^\circ\text{C}$  to 892.91  $\text{mg g}^{-1}$ . Thus, the temperature change had no practically significant effect on the iodine number. In this study, activation at  $450^\circ\text{C}$  was selected for the preparation of adsorbent. The ratio between DCS and  $\text{H}_3\text{PO}_4$  was set at 1:1.5, which gave the highest iodine number because the phosphate group increases the porosity of DCS-AC. This could be due to strong reaction of  $\text{H}_3\text{PO}_4$  with the surface carbon [24,25]. However, the decrease in iodine number of DCS-AC when the  $\text{H}_3\text{PO}_4$  proportion exceeds 1.5 is due to the phosphoric acid causing pore-size increase but decrease in specific surface [26]. The properties of DCS-AC activated by  $\text{H}_3\text{PO}_4$  at  $450^\circ\text{C}$  are shown in Table 2. The results show that DCS-AC treatment for 1 h gave the maximum iodine number of 889.57  $\text{mg g}^{-1}$ , which can be attributed to the reaction extent of  $\text{H}_3\text{PO}_4$  with surface carbon. The high iodine number can also be associated with a high adsorption capacity. Thus, the optimum conditions for the preparation of DCS-AC were treatment at  $450^\circ\text{C}$  for 1 h, and the ratio of DCS to  $\text{H}_3\text{PO}_4$  set at 1:1.5. This adsorbent was selected for the characterization and adsorption studies.

#### 3.2. Influence of preparation of PLA/DCS-AC

The formulation with polymer requires appropriate proportions. A PLA solution could not be formed at concentrations below 10 wt.%, but it was possible at 10 wt.%. The higher the PLA concentration, the poorer is access of dye to the activated carbon component. Therefore, a 10 wt.% concentration of PLA was considered the optimum. Table 3 shows the results from 10 wt.% PLA solution and DCS-AC powder in preparation of PLA/DCS-AC. The adsorption of iodine increased with AC content due to the availability of adsorption sites and increased carbon surface area [27]. The highest 587.43  $\text{mg g}^{-1}$  iodine number was obtained when PLA solution was mixed with DCS-AC powder at 5% wt., as the iodine number depends on the DCS-AC content in

PLA/DCS-AC. However, DCS-AC contents exceeding 5 wt.% were not possible.

3.3. Characterization of DCS-AC and PLA/DCS-AC

SEM were taken to study the morphology of the adsorbents. Fig. 2a–c shows the SEM images of the external surfaces of char, DCS-AC and PLA/DCS-AC, respectively, and Fig. 2d shows an internal cross-section of PLA/DCS-AC. DCS-AC and PLA/DCS-AC exhibited numerous pores on the surface, more than char. This confirms that the activation process increased porosity of the adsorbent. In addition, the pores were highly inter-connected in the cross-sectional image of PLA/DCS-AC.

The BET surface areas and total pore volumes of char, DCS-AC, and PLA/DCS-AC were determined by N<sub>2</sub> adsorption at 77 K using the BET model [28], and are summarized in Table 3. The results indicate that the activation increased BET surface area, and DCS-AC had a larger specific

surface than PLA/DCS-AC. Moreover, the BET surface area was directly proportional to the amount of adsorbed iodine, which was assumed to reflect the adsorption of Reactive Red 120. The BET surface areas of DCS-AC and PLA/DCS-AC were 230.96 and 190.30 m<sup>2</sup> g<sup>-1</sup>, respectively, which are significantly higher than those of granular activated carbon from porous carboxymethyl chitosan or of chitosan/Al<sub>2</sub>O<sub>3</sub>/Fe<sub>3</sub>O<sub>4</sub> beads (Table 4) [29–30].

It is well-known that the pores of adsorbents are generally divided into three groups: micropores (<2 nm), mesopores (2–50 nm), and macropores (>50 nm) [31]. The average pore diameters of DCS-AC and PLA/DCS-AC were 2.86 and 2.90 nm, respectively, in the mesopore range and with a relatively narrow pore-size distribution. The elemental compositions of char, DCS-AC and PLA/DCS-AC are summarized in Table 5. The carbon contents of char, DCS-AC, and PLA/DCS-AC were found to be 54.93, 56.16 and 56.12 wt.%, respectively.

The point of zero charge (pH<sub>pzc</sub>) was determined by the pH drift method, as shown in Fig. 3. Graphs were plotted of pH<sub>f</sub> and pH<sub>i</sub> for char, DCS/AC and PLA/DCS-AC. The pH<sub>pzc</sub> values of char, DCS/AC, and PLA/DCS-AC were 9, 3, and 4.5, respectively, indicating that DCS/AC and PLA/DCS-AC have positive charges that electrostatically repel the positively charged dye anions [32]. Thus, DCS-AC and PLA/DCS-AC were to adsorb Reactive Red 120 at the slightly elevated pH = 5.

The functional groups in DCS-AC, PLA, and PLA/DCS-AC were assessed from FT-IR spectra (Fig. 4). The band at about 3,300–3,500 cm<sup>-1</sup> was assigned to the O–H stretching vibrations. Moreover, the band at 1,600 cm<sup>-1</sup> was assigned to the C=O stretching of keto-carbonyl groups [33]. These functional groups enhanced the binding between the adsorbent surfaces and the dye in solution, so that the dye was less

Table 1  
Influences of impregnation ratio and activation reagents of DCS-AC treated at 400°C, 450°C or 500°C for 1 h

Activation reagents (AR)	Impregnation ratio AC: AR	Iodine number (mg g <sup>-1</sup> )		
		400°C	450°C	500°C
H <sub>3</sub> PO <sub>4</sub>	1:0.5	580.45	621.24	622.43
	1:1.0	594.63	686.26	690.46
	1:1.5	745.34	892.91	893.21
	1:2.0	657.45	798.28	799.32
	1:2.5	281.32	292.62	292.98
	1:3.0	119.45	120.80	121.21
KOH	1:0.5	654.31	703.05	703.45
	1:1.0	592.56	621.24	623.34
	1:1.5	489.51	538.76	541.98
	1:2.0	456.89	490.62	492.45
	1:2.5	400.43	411.62	411.99
	1:3.0	142.47	156.06	157.34
ZnCl <sub>2</sub>	1:0.5	687.41	740.31	741.32
	1:1.0	600.49	672.74	672.89
	1:1.5	784.32	839.24	840.78
	1:2.0	600.11	639.22	640.81
	1:2.5	523.56	588.94	589.23
	1:3.0	189.79	201.27	203.54

Table 2  
Influences of 450°C treatments on DCS-AC activated by H<sub>3</sub>PO<sub>4</sub>

Adsorbent	Activation	Iodine number (mg g <sup>-1</sup> )
Char	–	302.90
	Refluxed 2 h	316.45
	Refluxed 4 h	542.80
DCS-AC/H <sub>3</sub> PO <sub>4</sub>	Burned 0.5 h	673.80
	Burned 1 h	889.57
	Burned 1.5 h	741.80
	Burned 2 h	519.84

Table 3  
Ratio of 10 %wt. PLA solution and AC content affected bead form adsorbent

PLA solution (g)	Weight of AC (g)	% wt. of AC	PLA/DCS-AC	Iodine number (mg g <sup>-1</sup> )
19.8	0.2	1%	✓	336.21
19.6	0.4	2%	✓	376.92
19.4	0.6	3%	✓	409.12
19.2	0.8	4%	✓	491.42
19.0	1.0	5%	✓	587.43
18.8	1.2	6%	✗	–

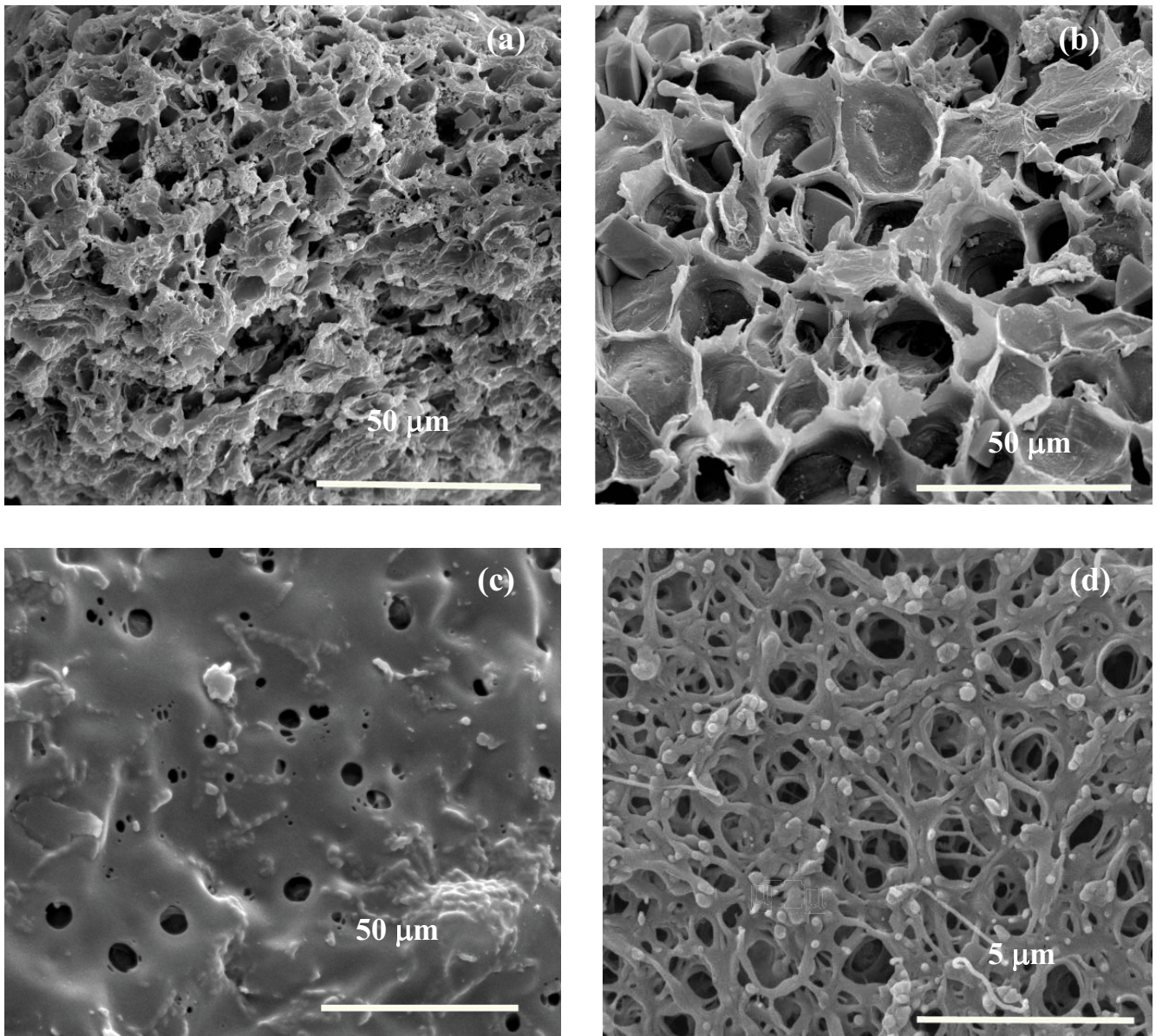


Fig. 2. SEM micrographs of (a) char, (b) DCS-AC, (c) PLA/DCS-AC and (d) cross-section of PLA/DCS-AC ( $\times 5,000$ ).

likely to escape. The functional groups on DCS-AC and PLA/DCS-AC didn't change the functional groups of PLA. The FT-IR spectrum of PLA/DCS-AC shows that the O–H band is blue shifted compared to pure PLA and DCS-AC. This could indicate the presence of DCS-AC in the PLA sphere.

### 3.4. Adsorption of Reactive Red 120 onto DCS-AC and PLA/DCS-AC

#### 3.4.1. Influences of contact time and initial Reactive Red 120 concentration

Fig. 5 shows the influences of contact time and initial Reactive Red 120 concentration on adsorption by DCS-AC and PLA/DCS-AC. From the results, the equilibrium times were around 24 h (0.10 g DCS-AC) and 36 h (0.30 g PLA/DCS-AC) at 30°C, pH 5, and initial Reactive Red 120

concentrations in 50–200 mg L<sup>-1</sup>. The amount adsorbed at equilibrium ( $q_e$ ) increased with the initial Reactive Red 120 concentration, as one would expect.

The effects of contact time relate to reaction kinetics modeled with pseudo-first-order [34] and pseudo-second-order [35] models. These were fit in the linearized forms shown in Eqs. (3) and (4), respectively.

$$\ln(q_e - q_t) = \ln q_e - k_1 t \quad (3)$$

$$\frac{t}{q_t} = \frac{1}{k_2 q_e^2} + \frac{1}{q_e} t \quad (4)$$

where  $q_e$  and  $q_t$  are the amounts of dye adsorbed (mg g<sup>-1</sup>) at equilibrium and at a given time  $t$ .  $k_1$  and  $k_2$  are the pseudo-first-order rate constant (min<sup>-1</sup>) and the pseudo-second-order

Table 4  
BET surface areas of char, DCS-AC, and PLA/DCS-AC, compared with chitosan beads

Sample	BET surface area (m <sup>2</sup> g <sup>-1</sup> )	Micropore volume (cm <sup>3</sup> g <sup>-1</sup> )	Average pore-size (nm)
Char	39.57	0.019	1.92
DCS-AC	230.96	0.107	2.86
PLA/DCS-AC	190.30	0.091	2.90
Porous carboxymethyl chitosan bead [29]	9.36	–	–
Chitosan/Al <sub>2</sub> O <sub>3</sub> /Fe <sub>3</sub> O <sub>4</sub> bead [30]	72.30	–	–

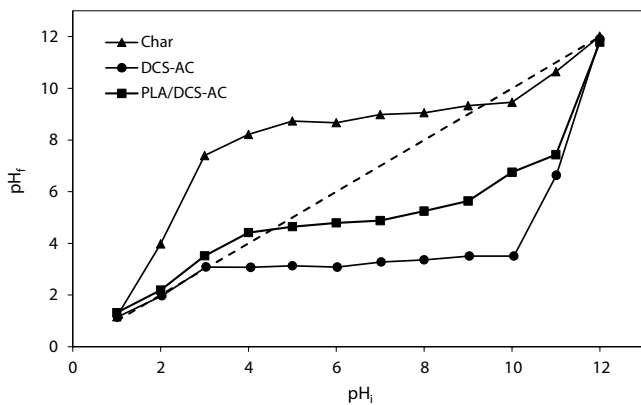


Fig. 3. Point of zero charge (pH<sub>pzc</sub>) for char, DCS-AC and PLA/DCS-AC.

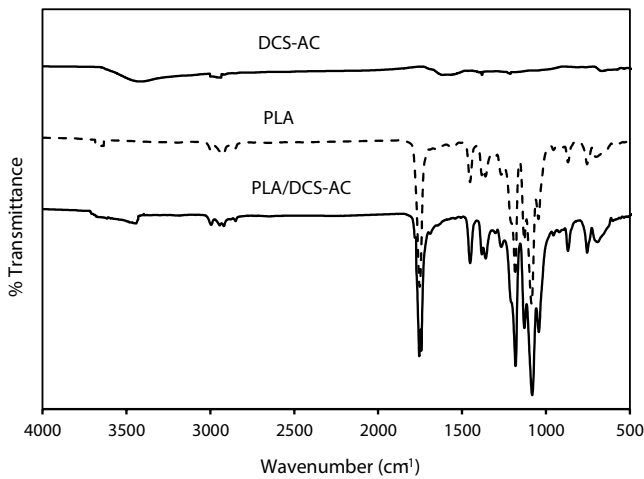


Fig. 4. FT-IR spectra of DCS-AC, PLA and PLA/DCS-AC.

rate constant (g mg<sup>-1</sup> min<sup>-1</sup>), respectively. The linear plots between ln(q<sub>e</sub> - q<sub>t</sub>) vs. t for the pseudo-first-order, and the linear plots of t/q<sub>t</sub> vs. t for pseudo-second-order adsorption kinetics are displayed in Fig. 6a–d. The values of k<sub>1</sub> and k<sub>2</sub> were obtained from slopes of the straight lines. The various kinetic parameters and the coefficient of determination R<sup>2</sup> are shown in Table 6. The results indicate that the kinetics of adsorption for Reactive Red 120 onto DCS-AC and PLA/DCS-AC were best fit by the pseudo-second-order model, based on R<sup>2</sup> being closest to one. The adsorption onto a porous solid could be separated into three stages:

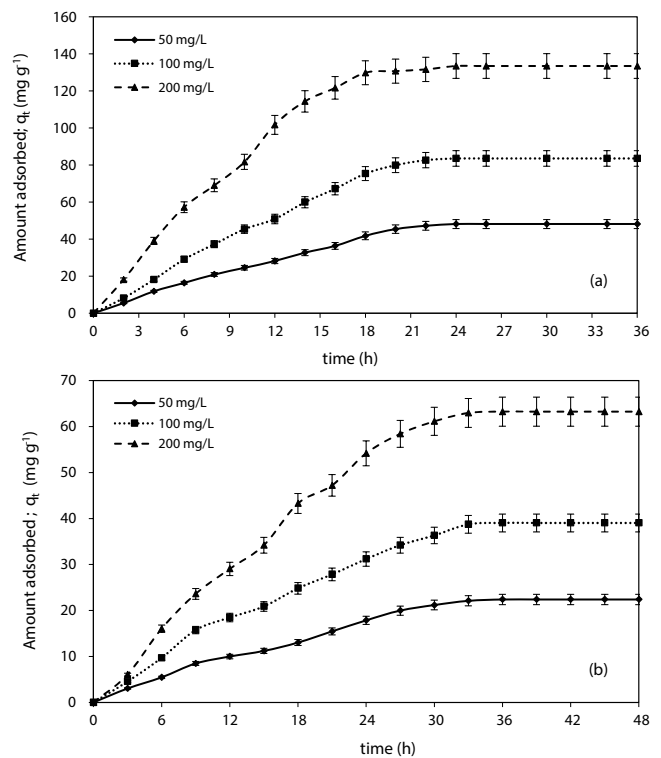


Fig. 5. Influences of contact time and initial Reactive Red 120 concentration on adsorption by DCS-AC and PLA/DCS-AC at 30°C and pH 5.0.

Table 5  
Elemental compositions of char, DCS-AC and PLA/DCS-AC

Sample	Elemental composition, wt. %				
	C	H	N	O	Ash
Char	54.93	3.63	0.02	36.71	4.71
DCS-AC	56.16	4.10	0.03	35.91	3.80
PLA/DCS-AC	56.12	4.57	0.02	34.76	4.53

external surface adsorption, gradual adsorption stage, and interior surface adsorption with final equilibrium stage [36].

### 3.4.2. Influences of amount of DCS-AC and PLA/DCS-AC

The doses of DCS-AC and PLA/DCS-AC from 0.10–0.60 g were used to study the influences of DCS-AC and

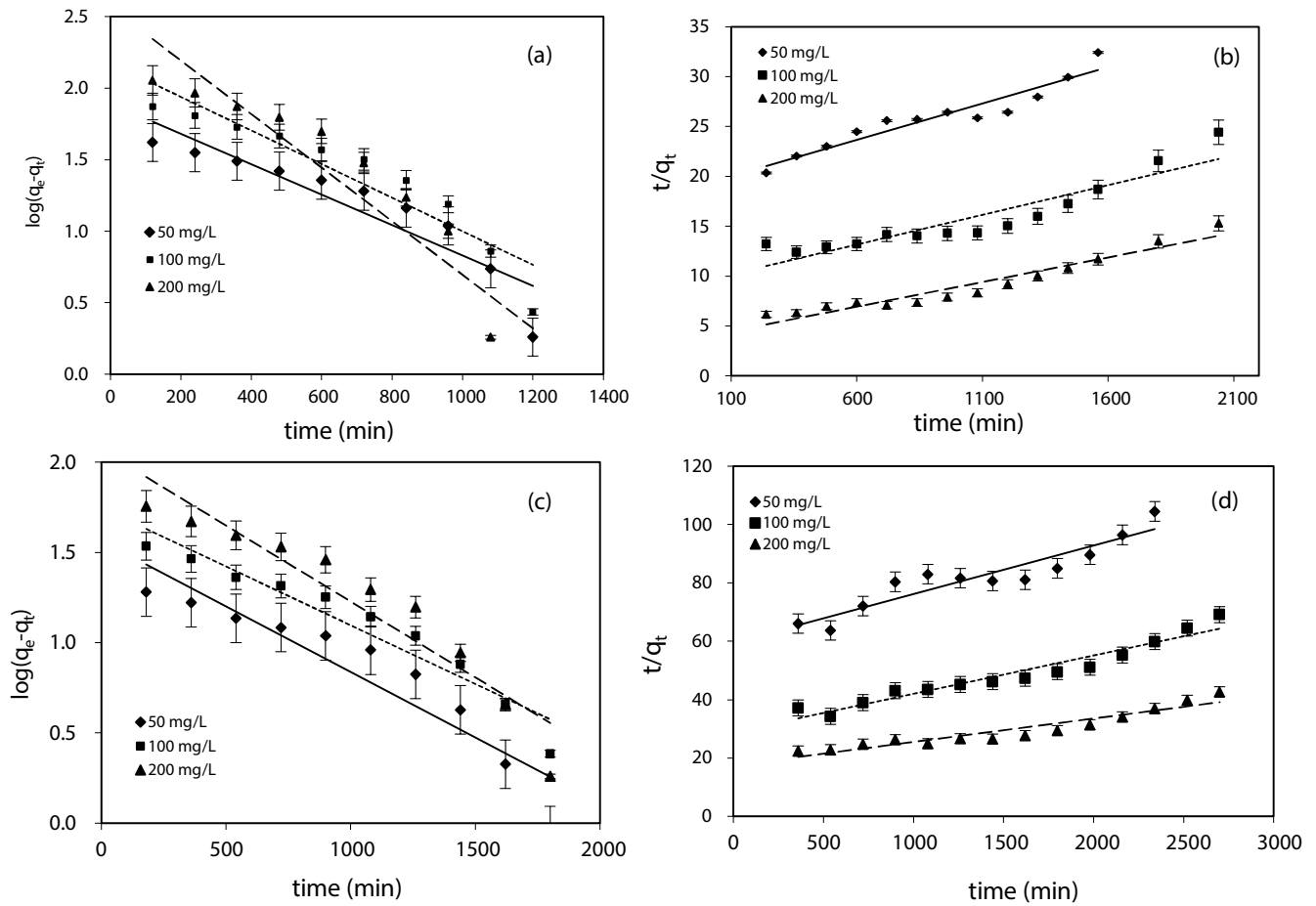


Fig. 6. Linearized plots of the kinetic adsorption models: pseudo-first-order (a,b), and pseudo-second-order (c,d), for Reactive Red 120 (50, 100 and 200 mg L<sup>-1</sup>) adsorption by DCS-AC and PLA/DCS-AC at 30°C and pH 5.0.

Table 6

Kinetic parameters in pseudo-first-order and pseudo-second-order models for Reactive Red 120 (50, 100 and 200 mg L<sup>-1</sup>) adsorption at 30°C by DCS-AC and PLA/DCS-AC, at pH 5.0.

DCS-AC							
C <sub>0</sub> (mg L <sup>-1</sup> )	q <sub>e(exp)</sub> (mg g <sup>-1</sup> )	Pseudo-first-order			Pseudo-second-order		
		q <sub>e</sub> (mg g <sup>-1</sup> )	k <sub>1</sub> (×10 <sup>-3</sup> ) (min <sup>-1</sup> )	R <sup>2</sup>	q <sub>e</sub> (mg g <sup>-1</sup> )	k <sub>2</sub> (×10 <sup>-5</sup> ) (g mg <sup>-1</sup> min <sup>-1</sup> )	R <sup>2</sup>
50	48.12	6.63	1.10	0.84	57.80	1.57	0.91
100	83.52	8.79	1.20	0.87	71.43	2.05	0.95
200	133.45	13.12	1.90	0.88	144.93	2.21	0.93
PLA/DCS-AC							
C <sub>0</sub> (mg L <sup>-1</sup> )	q <sub>e(exp)</sub> (mg g <sup>-1</sup> )	Pseudo-first-order			Pseudo-second-order		
		q <sub>e</sub> (mg g <sup>-1</sup> )	k <sub>1</sub> (×10 <sup>-4</sup> ) (min <sup>-1</sup> )	R <sup>2</sup>	q <sub>e</sub> (mg g <sup>-1</sup> )	k <sub>2</sub> (×10 <sup>-5</sup> ) (g mg <sup>-1</sup> min <sup>-1</sup> )	R <sup>2</sup>
50	37.90	4.75	6.04	0.86	51.81	2.64	0.87
100	62.19	5.75	7.01	0.82	62.51	2.61	0.93
200	86.85	7.84	8.01	0.89	147.06	3.28	0.91

PLA/DCS-AC dosage in the removal of 100 mg L<sup>-1</sup> of Reactive Red 120. The percentage of Reactive Red 120 at equilibrium increased with increasing DCS-AC and PLA/DCS-AC doses. However, the amount adsorbed at

equilibrium (q<sub>e</sub>) decreased with increasing DCS-AC and PLA/DCS-AC doses, as shown in Fig. 7. The results reflect the concept that an increase in adsorbent dosage increases the surface area and availability of adsorption sites [37]. The

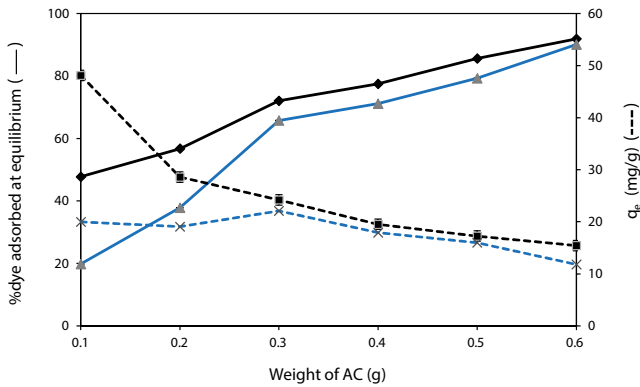


Fig. 7. Influence of dose of DCS-AC and PLA/DCS-AC for Reactive Red 120 (100 mg L<sup>-1</sup>) adsorption at 30°C, pH 5.0.

optimal dosages with the maximum of amount of adsorbed were 0.10 and 0.30 g for DCS-AC and PLA/DCS-AC, respectively. The highest amounts adsorbed at equilibrium were 48.12 mg g<sup>-1</sup> (DCS-AC) and 22.09 mg g<sup>-1</sup> (PLA/DCS-AC) and the equilibrations did not take a too long time for practical use.

### 3.4.3. Influence of pH

The pH of the solution affects the surface charges on the adsorbent, as well as the adsorbate species in solution. Influence of pH in the range 2–11 on adsorption of Reactive Red 120 by DCS-AC and PLA/DCS-AC is presented in Fig. 8. At pH below 6, an increase in the adsorption is due to the formation of protonated ions on surface, and an increase in adsorption capacity with a decrease in pH has also been reported from an adsorption study of reactive dye by Nopkhuntod et al. [38]. The increased adsorption of Reactive Red 120 ions on the surfaces of DCS-AC and PLA/DCS-AC is due to the protons electrostatically attraction sulfite ions onto DCS-AC and PLA/DCS-AC. The positive charge due to proton adsorption and protonation of functional groups improves adsorption by electrostatic attraction [39] when the pH of the solution is decreased. As the pH increases from 7 to 11, a decrease on the Reactive Red 120 adsorption capacity can be observed. At high pH values, the high concentrations of hydroxide ions charge the surfaces negatively and lead to repulsion of the anionic dye molecules.

### 3.4.4. Adsorption isotherms

Several model equations were tested for fit with the experimental adsorption isotherms. Langmuir, Freundlich, Temkin, and Dubinin–Radushkevich isotherms [40] are presented in linearized forms in Eqs. (5)–(8). The Langmuir isotherm [Eq. (5)] describes quantitatively the formation of a monolayer of adsorbate on the outer surface of the adsorbent, and assumes a uniform energy of adsorption [41]. The Freundlich isotherm [Eq. (6)] is commonly invoked to explain exponential adsorption of the target compound on heterogeneous surfaces [42, 43]. The Temkin isotherm [Eq. (7)] contains a factor that explicitly takes into account

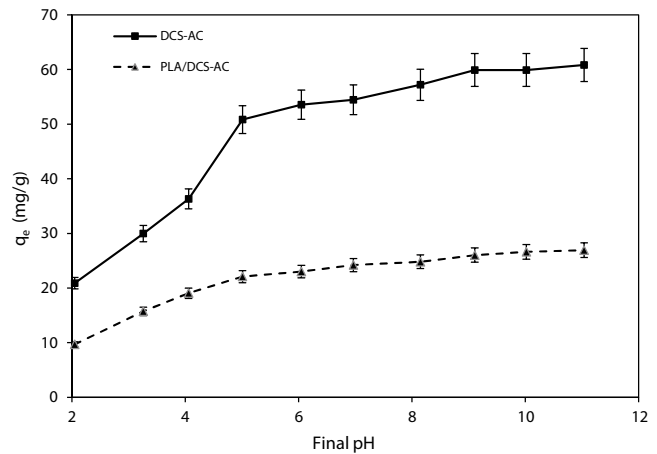


Fig. 8. Influences of pH on adsorption of Reactive Red 120 (100 mg L<sup>-1</sup>) by DCS-AC and PLA/DCS-AC in the pH range 2–11 at 30°C.

the adsorbent–adsorbate interactions and assumes the heat of adsorption of all molecules in the layer would decrease linearly rather than logarithmically with coverage. The derivation of this model is characterized by a uniform distribution of maximum binding energies [40]. The Dubinin–Radushkevich isotherm [Eq. (8)] is generally applied to express the adsorption mechanism with a Gaussian energy distribution on a heterogeneous surface [40,44].

$$\frac{C_e}{q_e} = \frac{1}{q_m b} + \frac{C_e}{q_m} \quad (5)$$

$$\log q_e = \log K_F + \frac{1}{n} \log C_e \quad (6)$$

$$q_e = B \ln A_i + B \ln C_e; B = \frac{RT}{b} \quad (7)$$

$$\ln q_e = \ln q_s - K_d \varepsilon^2; \varepsilon = RT \ln \left( 1 + \frac{1}{C_e} \right) \quad (8)$$

where  $C_e$  and  $q_e$  are the equilibrium concentration (mg L<sup>-1</sup>) and the amount adsorbed at equilibrium (mg g<sup>-1</sup>), respectively. The  $q_m$  and  $b$  are Langmuir parameters for the maximum adsorption capacity (mg g<sup>-1</sup>) and the adsorption equilibrium constant (L mg<sup>-1</sup>), respectively.  $K_F$  and  $n$  are Freundlich parameters indicating adsorption capacity (L g<sup>-1</sup>) and adsorption intensity, respectively. The  $A_i$  is Temkin isotherm equilibrium binding constant (L g<sup>-1</sup>),  $R$  is the universal gas constant (8.314 J mol<sup>-1</sup>K<sup>-1</sup>),  $T$  is absolute temperature (=298 K), and  $B$  is a constant related to the heat of sorption (J mol<sup>-1</sup>). The  $q_s$  is theoretical isotherm saturation capacity (mg g<sup>-1</sup>),  $K_d$  is Dubinin–Radushkevich isotherm constant (mol<sup>2</sup> kJ<sup>-2</sup>) and  $e$  is Dubinin–Radushkevich isotherm constant. The usual approach applied is to distinguish the physical and chemical adsorption by their mean free energies,  $E$  per molecule of adsorbate (for removing a molecule from its location in the sorption space to the infinity), which can be computed from Eq. (9) [45].

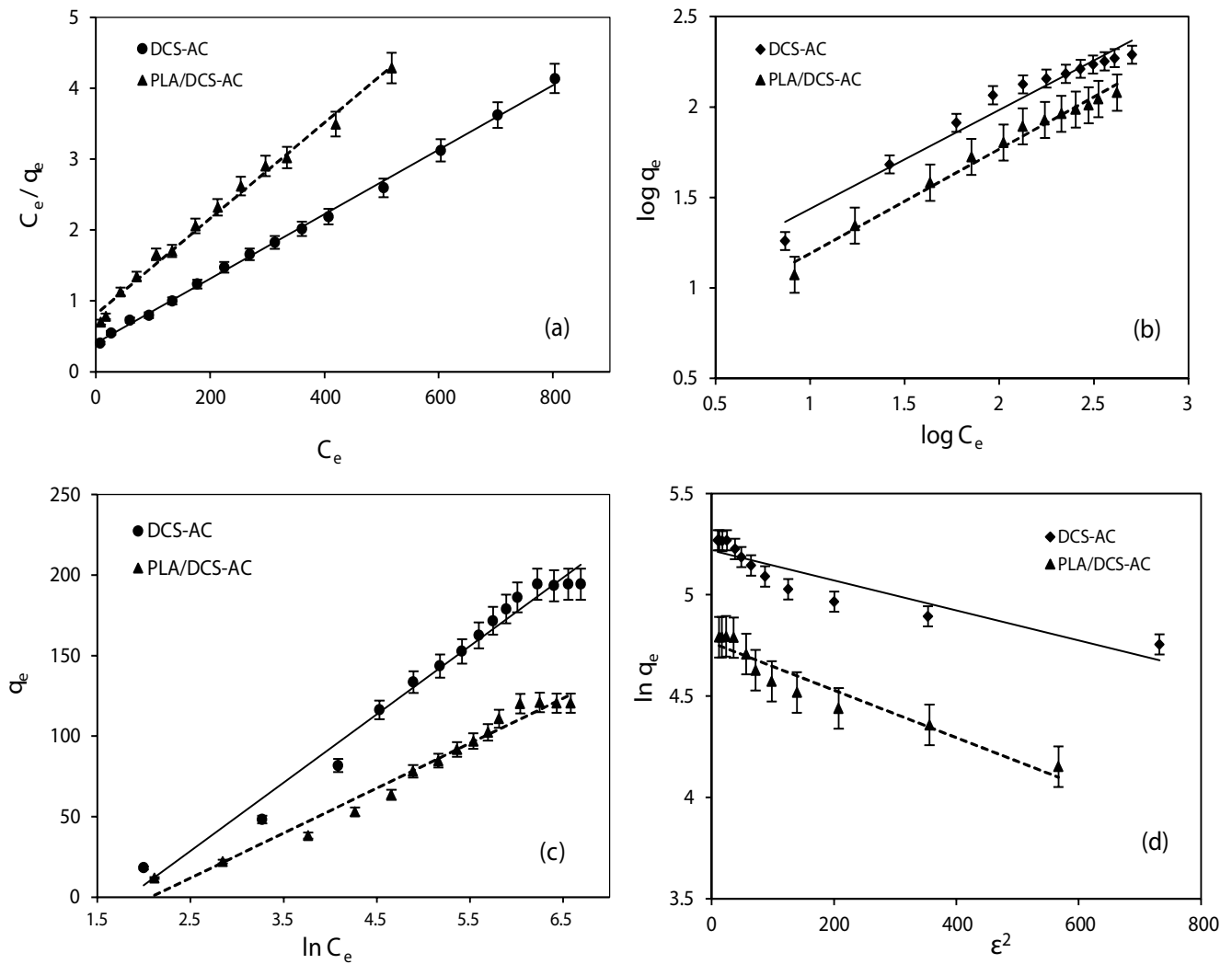


Fig. 9. Adsorption isotherm fits of (a) Langmuir, (b) Freundlich, (c) Temkin, and (d) Dubinin–Radushkevich for Reactive Red 120 adsorption onto DCS-AC and PLA/DCS-AC at 30°C, and pH 5.

Table 7

Isotherm parameters of Reactive Red 120 adsorption on DCS-AC and PLA/DCS-AC at pH 5, 30°C

Models	Parameter	DCS-AC	PLA/DCS-AC
Langmuir	$q_m$ (mg g <sup>-1</sup> )	222.22	147.06
	$b$ (L mg <sup>-1</sup> )	0.01	0.02
	$R^2$	0.99	0.99
Freundlich	$K_f$ (L g <sup>-1</sup> )	3.78	3.52
	$n$	1.62	1.12
	$R^2$	0.98	0.95
Temkin	$A_i$ (L g <sup>-1</sup> )	0.16	0.12
	$B$ (J mol <sup>-1</sup> )	42.43	27.89
	$R^2$	0.97	0.93
Dubinin–Radushkevich	$K_d$ (mol <sup>2</sup> kJ <sup>-2</sup> ) × 10 <sup>-3</sup>	0.7	1.2
	$q_s$ (mg g <sup>-1</sup> )	184.86	117.14
	$E$ (kJ mol <sup>-1</sup> )	0.36	0.21
	$R^2$	0.92	0.89

$$E = \frac{1}{\sqrt{2K_d}} \quad (9)$$

The fits with Langmuir, Freundlich, Temkin, and Dubinin–Radushkevich isotherms are shown in Fig. 9, and all isotherm parameters estimated from the slope and the intercept of the fitted straight line, along with the coefficient of determination  $R^2$ , are displayed in Table 7. The results indicate that data for the DCS-AC and PLA/DCS-AC were best fit with the Langmuir isotherm model, giving the highest  $R^2$ . This suggests monolayer adsorption according to Langmuir theory. The surface is relatively homogenous in terms of functional groups having significant interactions with Reactive Red 120 [43]. The maximum adsorption capacities ( $q_m$ ) of DCS-AC and PLA/DCS-AC for Reactive Red 120 were determined from the Langmuir equation were 222.22 and 147.06 mg g<sup>-1</sup>, respectively. Moreover, the Reactive Red 120 uptake maximum capacities ( $q_{m'}$ , mg g<sup>-1</sup>) of DCS-AC, along with those of other adsorbents reported in the literature, are given in Table 8. The  $q_m$  values of DCS-AC and PLA/DCS-AC were larger than those of other activated carbons prepared from biomass for the removal of Reactive Red 120.

### 3.4.5. Influences of temperature and thermodynamics

The influences of temperature on Reactive Red 120 (25 and 50 mg L<sup>-1</sup>) adsorption by DCS-AC and PLA/DCS-AC were assessed from testing the four temperatures 30°C, 40°C, 50°C and 60°C. The van't Hoff Eq. (10) suggested plotting  $\ln K_c$  vs.  $1/T$  as shown in Fig. 10. Thus, enthalpy ( $\Delta H^\circ$ ) and entropy ( $\Delta S^\circ$ ) were estimated from slope and intercept of the linear fit, and the Gibb's free energy ( $\Delta G^\circ$ ) was determined by Eq. (11) [52].

$$\ln K_c = \frac{\Delta S^\circ}{R} - \frac{\Delta H^\circ}{RT} \quad (10)$$

$$\Delta G^\circ = \Delta H^\circ - T\Delta S^\circ \quad (11)$$

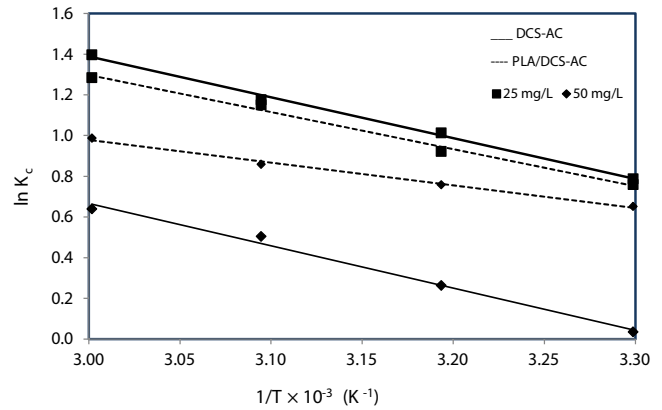


Fig. 10. van't Hoff plot for Reactive Red 120 (25 and 50 mg L<sup>-1</sup>) on DCS-AC and PLA/DCS-AC at 30°C, 40°C, 50°C and 60°C, pH 5.0.

where  $K_c$  is the ratio of  $C_A$  (the solid-phase concentration of Reactive Red 120 at equilibrium in mg L<sup>-1</sup>) to  $C_e$  (the equilibrium concentration of Reactive Red 120 in solution in mg L<sup>-1</sup>),  $R$  is the universal gas constant (8.314 J K<sup>-1</sup> mol<sup>-1</sup>), and  $T$  is the absolute temperature (K).

The thermodynamic parameter estimates are summarized in Table 9. The positive values of  $\Delta H^\circ$  and  $\Delta S^\circ$  indicate an endothermic process, and the degree of randomness at the solid–liquid interface increases with adsorption of Reactive Red 120 on both DCS-AC and PLA/DCS-AC. The negative values of  $\Delta G^\circ$  at all temperatures confirm the thermodynamic feasibility and spontaneity of these adsorption processes [53].

### 3.4.6 Application to treatment of batik wastewater

The DCS-AC and PLA/DCS-AC were tested on textile wastewater obtained from batik handicraft group (Raya batik community enterprise) in Yarang, Pattani, Thailand. Reactive Red 120 adsorptions from batik wastewater on DCS-AC and PLA/DCS-AC were found to be 75.12% and 64.04%, respectively. This confirmed that DCS-AC and

Table 8  
Maximum adsorption capacities of Reactive Red 120 compared with prior literature data

No.	Adsorbent	pH	$q_m$ (mg g <sup>-1</sup> )	Ref.
1.	Activated carbon from cumin	2.0	47.88	[14]
2.	<i>Saccharomyces cerevisiae</i> yeast	5.0	23.48	[15]
3.	Nano alumina powder	3.0	65.23	[46]
4.	Chitosan bead	5.0	129.9	[47]
5.	<i>Spirulina platensis</i> (SP)		SP = 482.2	
	Commercial activated carbon (AC)	2.0	AC = 267.2	[48]
6.	Cross-linked chitosan-epichlorohydrin biobeads	5.0	81.3	[49]
7.	Chitosan–octadecylamine	5.0	5.6	[50]
8.	Bentonite modified by cetyltrimethylammonium bromide	5.0	51.28	[51]
9.	DCS-AC	5.0	222.22	
	PLA/DCS-AC	5.0	147.06	This study

Table 9

Thermodynamic parameters for Reactive Red 120 (25 and 50 mg L<sup>-1</sup>) on DCS-AC and PLA/DCS-AC at 30°C–60°C, pH 5

Adsorbents	C <sub>0</sub> (mg L <sup>-1</sup> )	Thermodynamic parameters					
		-ΔG° (kJ mol <sup>-1</sup> ) at different T (K)				ΔH° (kJ mol <sup>-1</sup> )	ΔS° × 10 <sup>-2</sup> (kJ mol <sup>-1</sup> K <sup>-1</sup> )
		303	313	323	333		
DCS-AC	25	1.99	2.61	3.22	3.84	16.69	6.16
	50	0.11	0.68	1.26	1.83	17.28	5.74
PLA/DCS-AC	25	1.89	2.46	3.02	3.58	15.16	5.64
	50	1.62	1.98	2.34	2.71	19.28	3.62

PLA/DCS-AC can serve as alternative adsorbents for use by the batik handicraft group in the small community.

#### 4. Conclusions

In this study the capability of DCS-AC and PLA/DCS-AC to act as an efficient and eco-friendly sorbent for removing Reactive Red 120 from wastewater was demonstrated. The best isotherm fit to Reactive Red 120 adsorption on DCS-AC and PLA/DCS-AC was by the Langmuir isotherm model, and the  $q_m$  value estimates found were 222.22 and 147.06 mg g<sup>-1</sup>, respectively. The positive enthalpy of adsorption confirmed it was endothermic. The highest efficiencies of Reactive Red 120 adsorption in batik wastewater by DCS-AC and PLA/DCS-AC were about 75.12% and 64.04%, respectively. Therefore, the demonstrated DCS-AC and PLA/DCS-AC can serve as alternative adsorbents in the removal of dyes from wastewater.

#### Acknowledgments

The authors are grateful to the Department of Science, Faculty of Science and Technology, Prince of Songkla University, Pattani Campus, Thailand; and this research was supported by the Prince of Songkla University (PSU grant number SAT6202068S, Ref. Number: 22147). We are thankful to Assoc. Prof. Dr. Seppo Juhani Karrila for assistance with English language.

#### References

- [1] K. Kerdtthip, N. Laisatrakulaj, J. Vongphantuset, Modular batik stamp block: development of southern Thai printing batik stamp block, *Veridian E-J. Silpakorn Univ.*, 8 (2015) 127–142.
- [2] F. Rafii, W. Franklin, C.E. Cerniglia, Azoreductase activity of anaerobic bacteria isolated from human intestinal microflora, *Appl. Environ. Microbiol.*, 56 (1990) 2146–2151.
- [3] A.A. Dias, M.R. Bezerra, M.P. Lemos, N.A. Pereira, In vivo and laccase-catalysed decolorization of xenobiotic azo dyes by a basidiomycetous fungus: characterization of its ligninolytic system, *World J. Microbiol. Biotechnol.*, 19 (2003) 969–975.
- [4] A. ElAziz A. Nayl, R.A. Elkhashab, T.E. Malah, S.M. Yakout, M.A. El-Khateeb, M.S.S. Ali, H.M. Ali, Adsorption studies on the removal of COD and BOD from treated sewage using activated carbon prepared from date palm waste, *Environ. Sci. Pollut. Res.*, 24 (2017) 22284–22293.
- [5] I. El Saliby, L. Erdei, J.-H. Kim, H. Kyong Shon, Adsorption and photocatalytic degradation of methylene blue over hydrogen-titanate nanofibres produced by a peroxide method, *Water Res.*, 47 (2013) 4115–4125.
- [6] G. Vijayaraghavan, S. Shanthakumar, Effective removal of Reactive Magenta dye in textile effluent by coagulation using algal alginate, *Desal. Water Treat.*, 121 (2018) 22–27.
- [7] W. Yilin, L. Chunxiang, M. Minjia, L. Peng, L. Xinlin, Y. Yongsheng, Fabrication and evaluation of GO/TiO<sub>2</sub>-based molecularly imprinted nanocomposite membranes by developing a reformative filtering strategy: application to selective adsorption and separation membrane, *Sep. Purif. Technol.*, 212 (2019) 245–254.
- [8] T.-H. Liou, Development of mesoporous structure and high adsorption capacity of biomass-based activated carbon by phosphoric acid and zinc chloride activation, *Chem. Eng. J.*, 158 (2010) 129–142.
- [9] C. Sagnik, C. Shamik, D.S. Papita, Adsorption of crystal violet from aqueous solution onto NaOH-modified rice husk, *Carbohydr. Polym.*, 86 (2011) 1533–1541.
- [10] S. Lairini, K. El Mahtal, Y. Miyah, K. Tanji, S. Guissi, S. Boumchita, F. Zerrouq, The adsorption of crystal violet from aqueous solution by using potato peels (*Solanum tuberosum*): equilibrium and kinetic studies, *J. Mater. Environ. Sci.*, 8 (2013) 3252–3261.
- [11] F. Hayeeye, M. Sattar, S. Tekasakul, O. Sirichote, Adsorption of rhodamine B on activated carbon obtained from pericarp of rubber fruit in comparison with the commercial activated carbon, *Songklanakarin J. Sci. Technol.*, 36 (2014) 177–187.
- [12] K. Saeed, M. Ishaq, S. Sultan, I. Admad, Removal of methyl violet 2-B from aqueous solutions using untreated and magnetite-impregnated almond shell as adsorbents, *Desal. Water Treat.*, 57 (2016) 13484–13493.
- [13] M.A. Hossein, H. Behzad, Removal of Reactive Red 120 and Direct Red 81 dyes from aqueous solutions by Pumice, *Res. J. Chem. Environ.*, 16 (2012) 62–68.
- [14] E. Bazrafshan, M. Ahmadabadi, A.H. Mahvi, Reactive red-120 removal by activated carbon obtained from cumin herb wastes, *Fresenius Environ. Bull.*, 22 (2013) 584–590.
- [15] A. Navaei, M. Yazdani, H. Alidadi, M. Dankoob, Z. Bonyad, A. Dehghan, A. Hosseini, Biosorption of Reactive Red 120 dye from aqueous solution using *Saccharomyces cerevisiae*: RSM analysis, isotherms and kinetic studies, *Desal. Water Treat.*, 171 (2019) 418–427.
- [16] C.A. Smolders, A.J. Reuvers, R.M. Boom, I.M. Wienk, Microstructures in phase-inversion membranes. Part 1. Formation of macrovoids, *J. Membr. Sci.*, 73 (1992) 259, doi: 10.1016/0376-7388(92)80134-6.
- [17] M. Sattar, F. Hayeeye, W. Chinpa, O. Sirichote, Poly(lactic acid)/activated carbon composite beads by phase inversion method for kinetic and adsorption studies of Pb<sup>2+</sup> ions in aqueous solution, *Desal. Water Treat.*, 146 (2019) 227–235.
- [18] M. Sattar, F. Hayeeye, W. Chinpa, O. Sirichote, Preparation and characterization of poly(lactic acid)/activated carbon composite bead via phase inversion method and its use as adsorbent for Rhodamine B in aqueous solution, *J. Environ. Chem. Eng.*, 5 (2017) 3780–3791.
- [19] P.A. Philadelphia, Annual Book of ASTM Standards, Standard Test Method for Determination of Iodine Number of Activated Carbon, ASTM D4607-94, United States of America, 2006.

- [20] Y.F. Jia, B. Xiao, K.M. Thomas, Adsorption of metal ions on nitrogen surface functional groups in activated carbons, *Langmuir*, 18 (2002) 470–478.
- [21] F. Hayeeye, M. Sattar, W. Chinpa, O. Sirichote, Kinetics and thermodynamics of Rhodamine B adsorption by gelatin/activated carbon composite beads, *Colloids Surf., A*, 513 (2017) 259–266.
- [22] J. Rahchamani, H. Zavvar Mousavi, M. Behzad, Adsorption of methyl violet from aqueous solution by polyacrylamide as an adsorbent: isotherm and kinetic studies, *Desalination*, 267 (2011) 256–260.
- [23] G.L. Puma, A. Bono, D. Krishnaiah, J.G. Collin, Preparation of titanium dioxide photocatalyst loaded onto activated carbon support using chemical vapor deposition: a review paper, *J. Hazard. Mater.*, 157 (2008) 209–219.
- [24] H. Deng, G. Li, H. Yang, J. Tang, J. Tang, Preparation of activated carbons from cotton stalk by microwave assisted KOH and  $K_2CO_3$  activation, *Chem. Eng. J.*, 163 (2010) 373–381.
- [25] C. Saka, BET, TG–DTG, FT-IR, SEM, iodine number analysis and preparation of activated carbon from acorn shell by chemical activation with  $ZnCl_2$ , *J. Anal. Appl. Pyrolysis*, 95 (2012) 21–24.
- [26] G.O. El-Sayed, M.M. Yehia, A.A. Asaad, Assessment of activated carbon prepared from corncob by chemical activation with phosphoric acid, *Water Resour. Ind.*, 7 (2014) 66–75.
- [27] A. Mianowski, M. Owczarek, A. Marecka, Surface area of activated carbon determined by the iodine adsorption number, *Energy Sources Part A*, 29 (2007) 839–850.
- [28] S. Brunauer, J. Skalny, E.E. Bodor, Adsorption on nonporous solids, *J. Colloid Interface Sci.*, 30 (1969) 546–552.
- [29] W. Luo, Z. Bai, Y. Zhu, Fast removal of Co(II) from aqueous solution using porous carboxymethyl chitosan beads and its adsorption mechanism, *RSC Adv.*, 8 (2018) 13370–13387.
- [30] F. Bozorgpour, H.F. Ramandi, P. Jafari, S. Samadi, S.S. Yazd, M. Aliabadi, Removal of nitrate and phosphate using chitosan/ $Al_2O_3/Fe_3O_4$  composite nanofibrous adsorbent: comparison with chitosan/ $Al_2O_3/Fe_3O_4$  beads, *Int. J. Biol. Macromol.*, 93 (2016) 557–565.
- [31] U. Kuila, M. Prasad, Specific surface area and pore-size distribution in clays and shales, *Geophys. Prospect.*, 62 (2013) 341–362.
- [32] F. Hayeeye, M. Sattar, Removal of crystal violet in aqueous solution by activated carbon from the pericarp of rubber fruit and bagasse: kinetics, thermodynamics and adsorption studies, *Desal. Water Treat.*, 202 (2020) 420–434.
- [33] B. Stuart, *Infrared Spectroscopy: Fundamentals and Applications*, John Wiley & Sons Ltd., University of Technology, Sydney, Australia, 2004.
- [34] S. Lagergren, Zur theorie der sogenannten adsorption gelöster stoffe, *Kungliga Svenska Vetenskapsakademiens Handlingar*, 24 (1898) 1–39.
- [35] Y.S. Ho, G. McKay, Pseudo-second-order model for sorption processes, *Process Biochem.*, 34 (1999) 451–465.
- [36] M. Ghaedi, A.M. Ghaedi, E. Negintaji, A. Ansari, A. Vafaei, M. Rajabi, Random forest model for removal of bromophenol blue using activated carbon obtained from *Astragalus bisulcatus* tree, *J. Ind. Eng. Chem.*, 20 (2014) 1793–1803.
- [37] M. Ghaedi, A. Ansari, M.H. Habibi, A.R. Asghari, Removal of malachite green from aqueous solution by zinc oxide nanoparticle loaded on activated carbon: kinetics and isotherm study, *J. Ind. Eng. Chem.*, 20 (2014) 17–28.
- [38] S. Nopkhuntod, S. Dararat, J. Yimrattanabovorn, Removal of reactive dyes from wastewater by shale, *Songklanakarin J. Sci. Technol.*, 34 (2012) 117–123.
- [39] M. Ozacar, I. Sengil, Adsorption of reactive dyes on calcined alunite from aqueous, *J. Hazard. Mater.*, 98 (2003) 211–224.
- [40] A.O. Dada, A.P. Olalekan, A.M. Olatunya, O. Dada, Langmuir, Freundlich, Temkin and Dubinin–Radushkevich isotherms studies of equilibrium sorption of  $Zn^{2+}$  unto phosphoric acid modified rice husk, *IOSR J. Appl. Chem.*, 3 (2012) 38–45.
- [41] I. Langmuir, The adsorption of gases on plane surfaces of glass, mica and platinum, *J. Am. Chem. Soc.*, 40 (1918) 1361–1403.
- [42] H. Freundlich, Ueber Kolloidfällung and Adsorption, *Zeitschrift für Chemie und Industrie der Kolloide*, 1 (1907) 321–331.
- [43] S. Arabzadeh, M. Ghaedi, A. Ansari, F. Taghizadeh, M. Rajabi, Comparison of nickel oxide and palladium nanoparticle loaded on activated carbon for efficient removal of methylene blue: kinetic and isotherm studies of removal process, *Hum. Exp. Toxicol.*, 34 (2015) 153–169.
- [44] M.M. Dubinin, The potential theory of adsorption of gases and vapors for adsorbents with energetically non-uniform surface, *Chem. Rev.*, 60 (1960) 235–266.
- [45] J.P. Hobson, Physical adsorption isotherms extending from ultra-high vacuum to vapor pressure, *J. Phys. Chem.*, 73 (1969) 2720–2727.
- [46] K. Nadafi, M. Vosoughi, A. Asadi, M. Omidvar Borna, M. Shirmardi, Reactive Red 120 dye removal from aqueous solution by adsorption on nano-alumina, *J. Water Chem. Technol.*, 36 (2014) 125–133.
- [47] N. Mubarak, A.H. Jawad, W.I. Nawawi, Equilibrium, kinetic and thermodynamic studies of Reactive Red 120 dye adsorption by chitosan beads from aqueous solution, *Energy Ecol. Environ.*, 2 (2017) 85–93.
- [48] N.F. Cardoso, E.C. Lima, B. Royer, M.V. Bach, G.L. Dotto, L.A. Pinto, T. Calvete, Comparison of *Spirulina platensis* microalgae and commercial activated carbon as adsorbents for the removal of Reactive Red 120 dye from aqueous effluents, *J. Hazard. Mater.*, 241–242 (2012) 146–153.
- [49] A.H. Jawad, N.S. Mubarak, S. Sabar, Adsorption and mechanism study for Reactive Red 120 dye removal by cross-linked chitosan-epichlorohydrin bio beads, *Desal. Water Treat.*, 164 (2019) 378–387.
- [50] S. Kittinaovarat, P. Kansomwan, N. Jiratumnukul, Chitosan/modified montmorillonite beads and adsorption Reactive Red 120, *Appl. Clay Sci.*, 48 (2010) 87–91.
- [51] H.F. Al Rubai, A.K. Hassan, M.S. Sultan, W.M. Abood, Kinetics of adsorption of Reactive Red 120 using bentonite modified by CTAB and study the effect of salts, *Nat. Environ. Pollut. Technol.*, 20 (2021) 281–289.
- [52] A. Özcan, E. Mine Öncü, A. Safa Özcan, Kinetics, isotherm and thermodynamic studies of adsorption of acid blue 193 from aqueous solutions onto natural sepiolite, *Colloids Surf., A*, 277 (2006) 90–97.
- [53] N.M. Mahmoodi, Equilibrium, kinetics, and thermodynamics of dye removal using alginate in binary systems, *J. Chem. Eng. Data*, 56 (2011) 2802–2811.